Accepted Article Preview: Published ahead of advance online publication

Lensless single-shot multicore fiber endomicroscopy using a single multispectral hologram

Jakob Dremel, Elias Scharf, Sven Richter, Jurgen Czarske, and Robert Kuschmierz

Cite this article as: Jakob Dremel, Elias Scharf, Sven Richter, Jurgen Czarske, and Robert Kuschmierz. Lensless single-shot multicore fiber endomicroscopy using a single multispectral hologram. *Light: Advanced Manufacturing* accepted article preview 5 March, 2025; doi: 10.37188/lam.2025.027

Received 30 July 2024; revised 14 February 2024; accepted 4 March 2024; Accepted article preview online 5 March 2025

Lensless single-shot multicore fiber endomicroscopy using a single multispectral hologram

Jakob Dremel[1 2 3 *], Elias Scharf[1], Sven Richter[2 4], Jürgen Czarske[1 2 3 5 6 7], and Robert Kuschmierz[1 2 3]

[1] *Technische Universität Dresden, Laboratory of Measurement and Sensor System Technique, Dresden, Germany*
[2] *Technische Universität Dresden, Else Kröner Fresenius Center for Digital Health, Dresden, Germany*
[3] *Technische Universität Dresden, Competence Center BIOLAS, Dresden, Germany*
[4] *Technische Universität Dresden, Faculty of Medicine and University Hospital Carl Gustav Carus, Department of Neurosurgery, Dresden, Germany*
[5] *Technische Universität Dresden, Cluster of Excellence Physics of Life, Dresden, Germany*
[6] *Technische Universität Dresden, Institute of Applied Physics, Dresden, Germany*
[7] *University of Arizona, Wyant College of Optical Sciences, Tucson, USA*

*Correspondence to: Jakob Dremel: jakob.dremel@tu-dresden.de

Abstract

Endoscopes are indispensable for minimally invasive optical applications in medicine and production engineering. The smallest lensless endoscopes often use digital optics to compensate the intrinsic distortions of light propagation of multimode or multicore fibers. However, due to the wavelength dependency of the distortion, the approach is restricted to a narrow spectral range, which prevents multispectral imaging modalities. We employ a spatial light modulator with a high stroke above 2π, to generate a hologram which minimizes overall phase distortion for multiple spectral bands. This enables lensless multicore fiber single-shot RGB endoscopy, for the first time in the world. Many applications in advanced manufacturing and biomedicine such as in vivo tissue classification are enabled.

Minimally invasive endoscopy is highly relevant for biophotonic research for instance in neuroscience [1] and for minimally invasive medical applications for example in neurosurgery [2, 3] or inner ear surgery [4].

Normally, distal optics are used for fiber based endoscopy for (de-) magnification of the 2D image plane on the distal fiber facet [5, 6]. In the last decade multiple approaches based on correcting the inherent distortion of the light propagation through waveguides [7, 8, 9, 10] or core-wise scanning of a multicore fiber [11, 12] have been demonstrated showing significant advances towards ultra-thin lensless endoscopes. These systems work without optics at the distal end and are also named lensless endoscopes. On the one hand data driven approaches rely on inverting the complex light distortion during propagation based on learned examples in post processing [13, 14, 15, 16, 17, 18, 19]. On the other hand, physic based approaches rely on measuring the optical transfer function (OTF), most commonly via digital holography [20] and using spatial light modulator (SLM) for digital optical phase conjugation (DOPC), subsequently [21, 22]. The fiber is illuminated with the conjugate of the wavefront distortion, which results in an undistorted wave at the fiber output. Multicore fibers (MCF) and multimode fibers (MMF) have been used. While MMFs are thinner and offer higher information density, MCFs exhibit only low order OTF changes upon bending and have less complex propagation characteristics benefiting from a strong memory effect [7, 23, 24]. Thus, variations of the input wave directly translates to the output and fast 3D scanning using adaptive optics on the proximal side is enabled [25]. Additionally, simplified calibration procedures become available [26, 27].

Special MCF designs have been proposed which offer an increased field of view, higher photon efficiency and bending

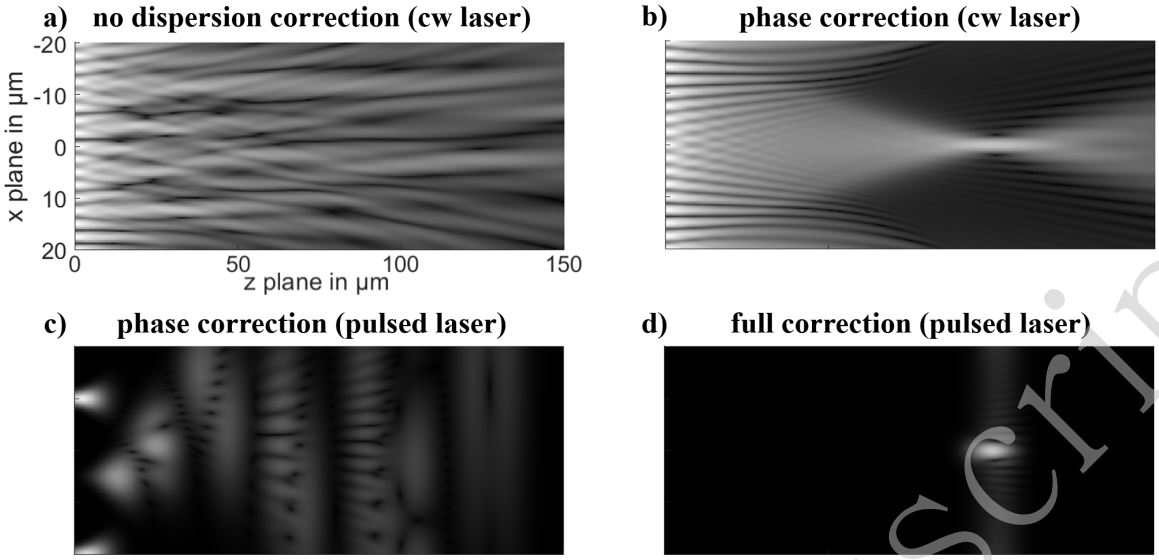

Fig. 1. Simulation: A converging beam couples into the proximal fiber facet. A Snapshot of the resulting intensity at the distal fiber end is shown for different light sources and different corrections. Top row: A narrow band continuous wave (cw) laser source is used. a) Due to intercore dispersion, the phase is scrambled and a speckle pattern results without a focus. b) For a narrow linewidth source phase correction within a maximum stroke of 2π enables focusing. Bottom row: A broadband cw or ultra-short pulsed light source is used. c) With phase correction with a maximum stroke of 2π, dispersion impedes focusing and needs to be reduced below the coherence length or pulse length, d) to form a focus.

independent OTF [28, 29, 30, 31]. This enables distortion compensation via static single or multilayered holograms for compact and robust designs with reduced complexity [32, 33]. Multiple minimally invasive applications have been enabled based on physical correction of the OTF in fibers such as label free Coherent anti-Stokes Raman scattering spectroscopy (CARS) endomicroscopy [34], endoscopic 3D printing [35], 2-photon excited fluorescence microscopy [36], laser ablation [37], photoacoustic endomicroscopy [38, 39] or single cell tomography using optical tweezers [40].

A major drawback of the proposed approaches compared to the state-of-the-art broadband lens-based imaging [41] is their narrow spectral range. Since, the wavefront distortion results from dispersion, the phase distortion is wavelength dependent. Thus, DOPC is only able to correct for a narrow spectral range around the operating wavelength. In principle, multispectral correction is feasible via Time Division Multiplexing (TDM), Space Division Multiplexing (SDM) or similar and was shown for multispectral focusing in scattering media such as tissue or MMF [42, 43, 44, 45]. These methods come with the cost of increased system complexity or reduced temporal resolution. Most significantly, TDM impedes the otherwise advantageous use of static 3D printed passive holograms. Furthermore, it prohibits the simultaneous correction of multiple wavelengths for instance for optogenetics [46] or label-free biomedical imaging like confocal fluorescence imaging or CARS endomicroscopy [47].

The underlying problem for lensless fiber endoscopy using MCFs is the scattering of effective refractive index n_{eff}, due to scattering in material properties and fiber geometry. This results in a scattering of the optical path length $l_{opt} = n_{eff} \cdot l$ which is proportional with the geometric fiber length l. The phase at the fiber output results to $\phi = 2\pi \cdot \mathrm{mod}(\frac{n_{eff} \cdot l}{\lambda}, 1)$. Considering a perfectly phase (but not length) corrected fiber at the design wavelength λ_D, a wavelength dependent phase distortion $\phi(\Delta\lambda) = 2\pi \cdot n_{eff} \cdot l \cdot \frac{\Delta\lambda}{\lambda_D^2}$ results, where $\Delta\lambda = \lambda - \lambda_D$. This means, the phase compensation deteriorates with increasing wavelength shifts $\Delta\lambda$ from the design wavelength, with increasing scattering of the effective refractive index and with increasing fiber length. The issue is sketched out in Fig. 1. Fig. 1a) shows the field if a MCF is illuminated with a coherent wave of wavelength λ_D. Dispersion induced phase distortion results in speckles in the far field. Fig. 1b) shows the field if the MCF is phase corrected. The individual beams interfere constructively to form a focus. Fig. 1c) shows the same phase corrected MCF again, but illuminated with a broadband wavelet centered around λ_D, with the bandwidth $\Delta\nu$. Only if the optical path length difference in the fiber is below the coherence length $L_c = \frac{2ln2}{\pi} \frac{\lambda_D^2}{n_{eff}\Delta\nu}$ or pulse length respectively constructive interference occurs, see Fig. 1d).

In order to gauge the issue for real fibers, σ_n was

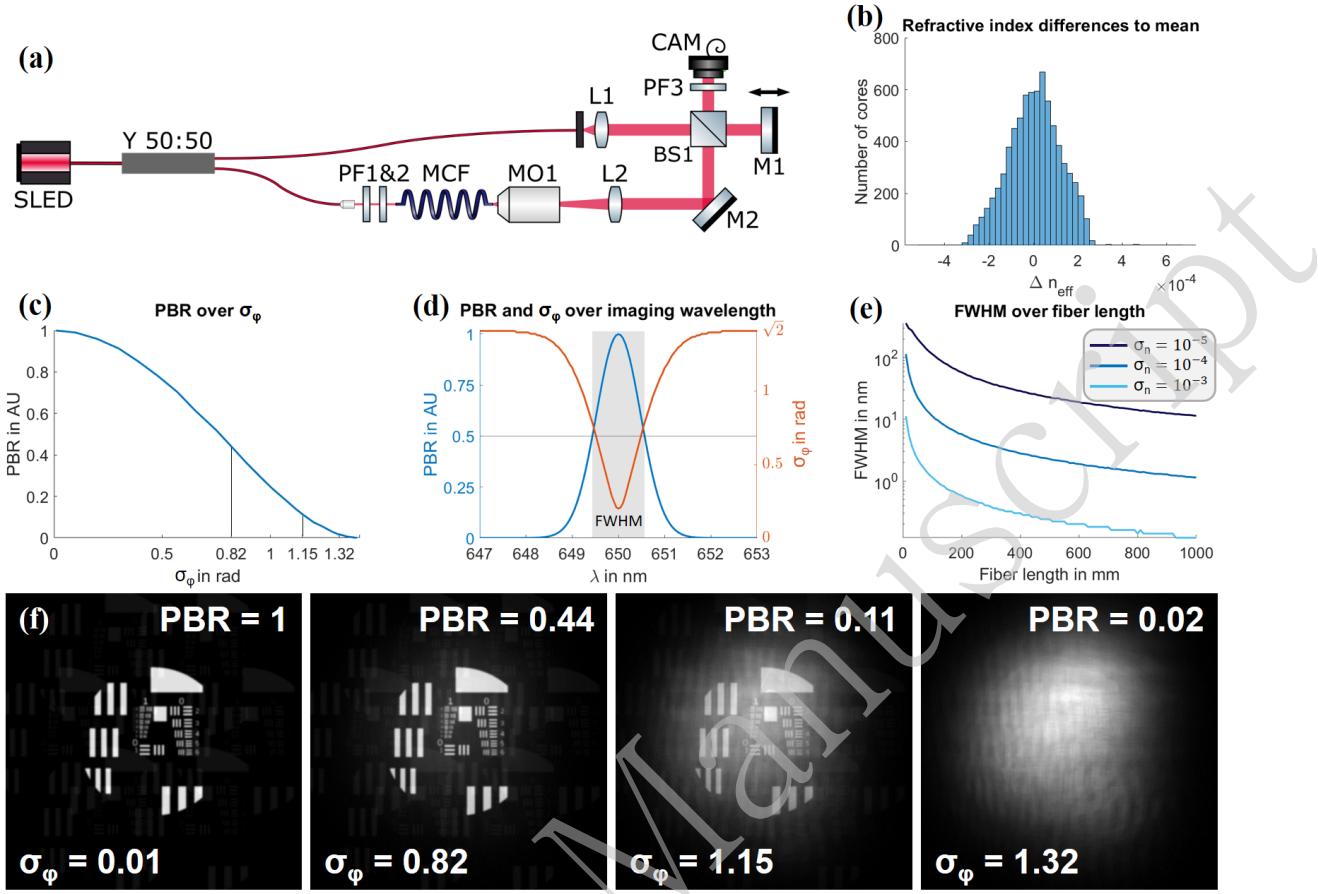

Fig. 2. a) White light interferometer to measure the intercore dispersion in a fiber bundle. B) Histogram of measured refractive index deviations of the commercial MCF. The standard deviation results to $\sigma_n = 10^{-4}$. c) Simulation: Focus quality measured in PBR in dependence of phase noise σ_ϕ. d) Simulation: Spectrally resolved PBR and σ_ϕ for the fiber with perfect phase correction for 650 nm. e) Simulation: FWHM for different fiber lengths calculated for different standard deviations of the refractive index. f) Simulated imaging with lensless endoscope using MCF with different corrections.

measured for a commercial MCF (Sumita HDIG, 10,000 cores, length 1 m) using a low coherence interferometer, see Fig. 2a). A fiber coupled super luminescent diode (SLED, $\lambda = 650\,\mathrm{nm}$, $\Delta\lambda = 6\,\mathrm{nm}$, Exalos, EXS210033-04) was used. A 50:50 fiber based y-coupler (Y 50:50, Thorlabs TW670R5A1) splits the light into the object and reference beam, respectively. The MCF was imaged onto a camera using a 20x microscope objective (MO1) and a tube lens (L2). Polarization filters (PF) were employed to adjust the relative amplitudes and to guarantee equal polarization of reference and object beam. The optical path length was measured by scanning the reference mirror M1 and a core wise evaluation of the interference fringe contrast in an off-axis hologram. Bending induced dispersion as well as aberrations of the reference beam were removed by lateral high pass filtering of the measured dispersion map. Fig. 2b) shows the distribution of the measured deviation of the refractive index Δn. A standard deviation of $\sigma_n \approx 10^{-4}$ results, meaning a 1 m long fiber exhibits a standard deviation of the optical path length of around $100\,\mu\mathrm{m}$. This limits the possible fiber length for non-linear endomicroscopy using ultra short laser pulses due to pulse broadening, for speckle-free broadband light sources, and correction of broadband fluorescenct light, for instance. This can be circumvented with advanced schemes with multiple SLMs for spatio-temporal beam shaping, increasing system complexity even further [48].

Based on the effective refractive index scattering the wavelength depended phase distortion can be calculated. The phase distortion is described by the standard deviation of the emitted phase which is $\sigma_\phi = 0$ for a perfectly corrected MCF, whereas a fully random MCF with equally distributed phase would result to $\sigma_\phi = \sqrt{2}$. The phase deviation limits the achievable imaging contrast, which is characterized by the peak-to-(mean)background ratio (PBR) [49]. Fig. 2c) shows the dependency PBR(σ_ϕ). Based on the measured Δn the resulting PBR was simulated for varying wavelengths assuming correction for $\lambda_c = 650\,\mathrm{nm}$. The measurement

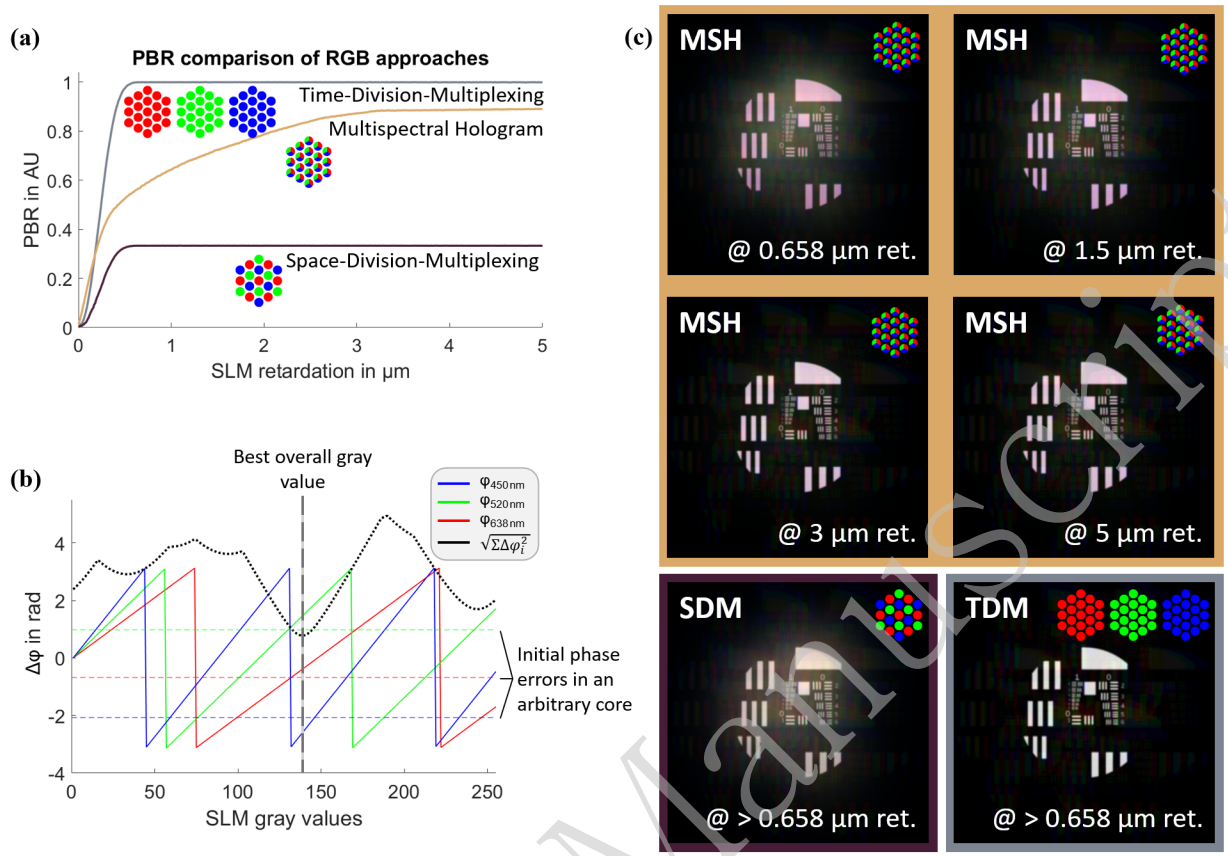

Fig. 3. A) Achievable PBR in dependency of SLM retardation for time division multiplex, multispectral holograms and space division holograms. The working principles are illustrated under each curve. B) Preliminary measured phase shifts for the different gray values of the SLM for different wavelengths (here the dependency is linearized, solid lines in red, green, and blue). Using this the gray value for each fiber core is calculated separately, it is the minimum of the MSE (black dotted line). The minimum of the MSE corrects all colors partially: a multispectral hologram. C) The simulated images compare the achievable image qualities using different max. retardations with an 8 bit SLM and an LED (MSH: Multispectral Hologram; SDM: Space-Division-Multiplexing; TDM: Time-Division-Multiplexing).

uncertainty was estimated in with $\sigma_{\phi_{meas}} \approx 0.2$ limiting the minimal phase distortion. We assumed wavelength independence of the refractive index, meaning no chromatic dispersion. An increased wavelength shift $\Delta\lambda$ increases the phase noise σ_ϕ, thus decreasing the PBR, see Fig. 2d). The width of the graph indicates the spectral range of the phase correction. This can be evaluated with the full width at half maximum (FWHM). The FWHM of $1.1\,\mathrm{nm}$ demonstrates that for the given fiber $\sigma_{l,opt}$ only narrow band imaging using DOPC is feasible. The spectral range can be increased by shortening the fiber or decreasing Δn as shown in Fig. 2e). In order to illustrate the influence of PBR on the resulting image, lensless imaging through a MCF with varying σ_ϕ was simulated using Fourier-optics, see Fig. 2f). As expected, image quality decreases with increasing phase deviation. However, Fig 2f) also shows, that imaging is feasible with non perfect phase correction.

Since, the phase stroke in SLM is wavelength dependent and can exceed 2π, multi spectral holograms with wavelength dependent phase patterns for partial phase correction can be generated [50]. Thus, multispectral imaging is feasible, in principle. In order to test this assumption a numerical simulation was performed using the single-shot imaging method proposed by Tsvirkun et al. [51], but any DOPC-based method could be used. The object is imaged with a microscope objective and tube lens on a camera. The phase-compensated MCF is put in between the object and the microscope objective, the objective focuses through the MCF. As the fiber facet is in between the object and Fourier plane the spatial resolution is no longer limited to the MCFs core count.

A fiber with $l = 0.1\,\mathrm{m}$, $\sigma_n \approx 10^{-4}$ and 10,000 cores was simulated by generating 10,000 Gaussian distributed core lengths. The resulting phase distortion was calculated for 3 wavelengths $\lambda_1 = 450\,\mathrm{nm}$; $\lambda_2 = 520\,\mathrm{nm}$; $\lambda_3 = 638\,\mathrm{nm}$, assuming no chromatic dispersion. A calibration

	TDM@ >0.658 µm	SDM@ >0.658 µm	MSH@ 0.658 µm	MSH@ 1.5 µm	MSH@ 3 µm
$\frac{FPS}{FPS_{TDM}}$	1	3	3	3	3
$\frac{PBR}{PBR_{TDM}}$	1	0.32	0.57	0.72	0.87

Table 1: Comparison of the simulation results for different maximal retardations.

measurement of this phase distortion was simulated to take measurement noise into account by adding Gaussian distributed phase values with $\sigma_{meas} = 0.2$. An SLM based DOPC was simulated. A linear dependency between SLM gray value and optical path length retardation was assumed. This means the phase retardation is wavelength dependent. The maximum stroke of the SLM was used as a variable within the simulation in order to estimate its influence.

Three different approaches for multispectral imaging are applied and compared:

- **Time Division Multiplexing (TDM):** An individual hologram per color is calculated. A sequential RGB source is used. The SLM is synchronized to the source, displaying the corresponding holograms. As an advantage, images are taken for every color and combined afterwards to one RGB image. Thus, an optimal compensation is enabled independent of the wavelength, see Fig. 3a) (gray). As a disadvantage, TDM requires dynamic, time depended holograms. Thus, imaging modalities requiring simultaneous multispectral illumination or detection such as confocal fluorescence microscopy are not feasible. Additionally, robust and cheap static phasemask 3D printing is inhibited. Furthermore, the imaging speed is limited by the switching time of the SLM and the number of color channels.

- **Space Division Multiplexing (SDM):** Each core is assigned to one of the colors. It is ensured that each color occurs with equal frequency and is evenly distributed on the fiber facet. The cores are then wavelength filtered according to their assigned color in a Bayer-pattern like filter. One static hologram is calculated where each core is compensated for their color. As an advantage, a static hologram can be employed. Thus, single-shot imaging becomes feasible if a multispectral lightsource is used. Additionally, imaging modalities requiring simultaneous multispectral illumination or detection such as confocal fluorescence microscopy can be realized. As a disadvantage, this limits the amount of available fiber cores N per wavelength. Consequently, it reduces the achievable PBR which scales linearly with $PBR \approx \frac{\pi N}{4}$ [49]. Thus, lower contrast images result.

- **multispectral Hologram (MSH):** One static hologram is calculated compensating all colors using all cores at the same time: For each core the merit function $\sqrt{\sum_1^3 \Delta\phi_i(S)^2}$ is minimized. Where S is the SLM gray value. The optimal gray value results in phase correction, that is descent for all wavelengths on average, see Fig. 3b). As an advantage, a static hologram can be employed and all fibers can be used for all wavelengths. Thus, single-shot imaging becomes feasible if a multispectral lightsource is used. Additionally, imaging modalities requiring simultaneous multispectral illumination or detection such as confocal fluorescence microscopy can be realized. As a disadvantage, the fibers are not corrected perfectly, reducing PBR. However, it is obvious in Fig. 3a) (yellow), that the image contrast increases with increasing stroke Δs. For $\Delta s = 1.1\,\mu\text{m}$ it doubles the achievable PBR compared to SDM and at $\Delta s = 1.7\,\mu\text{m}$ 75 % of maximum achievable PBR of TDM are reached.

The simulation results are summarized in Tab. 1. The frame rate (Frames-Per-Second, FPS) and the PBR as metric for the contrast are compared for the different methods normalized on the results of TDM FPS_{TDM} and PBR_{TDM}. TDM achieves the highest contrast but with the lowest frame rate. MSH is three-times faster than TDM with 87% of its contrast at 3 µm maximum retardation.

For experimental validation, a commercial MCF (Sumita HDIG, 10,000 cores, length 0.1 m) was calibrated multispectrally using a Mach-Zehnder interferometer, see Fig 4a). An RGB-laser was used (450 nm, 520 nm, 638 nm, FISBA READYBeam). The reference beam path (Fig. 4, yellow) uses a mirror on a stage to accommodate the fiber length. The object beam (Fig. 4, blue) passes the MCF. A x20 microscope objective and a tube lens image the distal fiber facet onto the SLM (Holoeye PLUTO-NIR-011, max. retardation 1.1 µm). The SLM is imaged via a 4f-system through a polarization filter on CAM1 (iDS UI-3482). The reference beam path is tilted in regards to the object beam for off-axis holography. Initially without a fiber, one calibration measurement per wavelength was taken to generate look-up-tables for the relationship "phase retardation – SLM gray value". After inserting the MCF, three phase measurements were taken sequentially for each wavelength to obtain the phase error for each core and for each color. Fig. 4b) shows

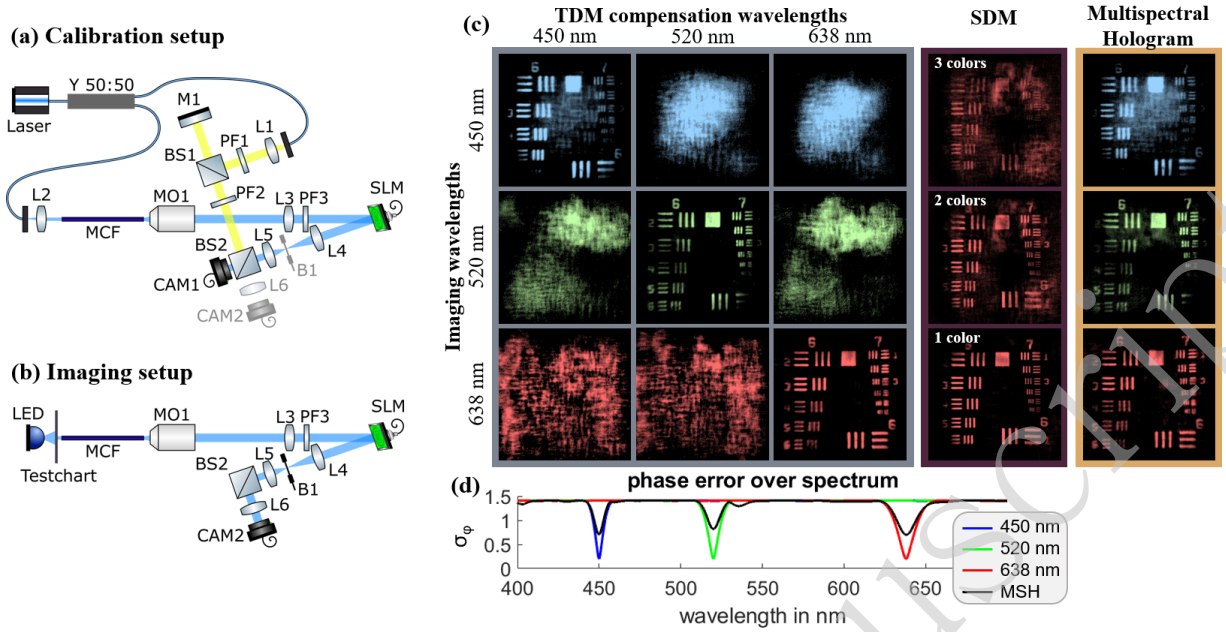

Fig. 4. a) Setup for calibration: Off-axis Mach-Zehnder interferometer is used for phase measurement. The reference beam is yellow, the object beam blue. b) Setup for imaging: The additional lens L6 images CAM2 in the far field of the MCF. c) Acquired images with sequential illumination & receiving beam forming using an SLM with a maximal retardation of 1.1 µm. The multispectral holograms allows imaging with all three wavelengths with a single hologram. d) Simulation: Comparison between three single spectral corrections at R, G, and B and a multi spectral correction.

the setup for testing and comparing the 3 different imaging schemes. A USAF-testchart is used as a reference object for imaging. The calibration laser is replaced with an RGB LED for illumination in transmission, see Fig. 4b). Using incoherent light is feasible due to the reduced fiber length as shown in Fig. 2. The testchart is placed 700 µm in front of the proximal fiber facet. From the R, G, and B calibration holograms the three correction schemes are calculated and displayed on the SLM. Images are recorded with CAM2 (iDS UI-3482) and displayed in Fig. 4c). **Results:**

- **Time Division Multiplexing:** The left cluster of 3x3 depicts the recorded image for each wavelength in dependence of the hologram used for correction. The holograms enable high contrast images, but only for their designated wavelengths. For different wavelengths the object becomes indistinguishable. The simulated graph underneath illustrates the wavelength dependency of the phase error of each hologram.
- **Space Division Multiplexing:** The effect of using a reduced number of fiber cores was implemented by angular filtering on the SLM. This means light from the filtered fiber cores was absorbed in the beam block B1. 3,300, 5,000, and all 10.000 fiber cores were chosen randomly to simulate SDM with 3, 2 colors, and 1 color respectably. Here, the red color channel is shown. It can be seen that the contrast reduced drastically with decreasing core number.
- **Multispectral Hologram:** Single-shot RGB imaging is enabled. As predicted by the simulation, the contrast is lower compared to TDM, but exceeds SDM significantly. Here the stroke was restricted to 1.1 µm. The contrast could be improved further, using a higher stroke SLM.

Lensless MCF endoscopy is promising for minimally invasive applications. The inherent narrow band principle limits applications however. We compared different approaches to enable multispectral lensless MCF endoscopy. Time division multiplexing maximizes the achievable imaging contrast, at the cost of a reduced frame rate and it does not enable modalities requiring simultaneous multispectral correction. Space Division Multiplexing is single-shot but greatly reduces imaging contrast. However, multispectral static holograms enable lensless single-shot multispectral endoscopy with a slightly diminished contrast. We demonstrated RGB imaging using a commercial SLM. However, further modalities relying on simultaneous multispectral phase correction can be enabled by static holograms as well. For instance CARS or confocal fluorescence endomicroscopy are enabled and can enhance diagnostic value, for instance in tissue differentiation. Additionally, employing a static multispectral correction enables using 3D printed holograms. These can be applied

directly onto the fiber facet using two-photon polymerization in order decrease system complexity and price, and to increase robustness. To further improve the image quality a broadband dispersion correction needs to be implemented. Using metasurfaces or multiple DOEs is a promising direction [52, 48]. For translation to the clinic, it is necessary to show that the multispectral approach also works with static DOEs, due to the required low maintenance and low failure rates. Many procedures would benefit from the endoscope's small form-factor, like neurosurgical or inner-ear surgeries.

Acknowledgement

Funding by Deutsche Forschungsgesellschaft (DFG Cz55/47-1), by the German Federation of Industrial Research Associations (AiF 21802 BG), the European Regional Development Fund (ERDF), and the Development Bank of Saxony (SAB) is gratefully acknowledged.

Conflict of interest

The authors declare no conflicts of interest.

Contributions

We want to thank Elisabeth Berkholz, Leon Stiffel and Dr. Martin Kroll for their valuable support.

References

[1] Accanto, N. et al. A flexible two-photon fiberscope for fast activity imaging and precise optogenetic photostimulation of neurons in freely moving mice. *Neuron* **111**, 176–189.e6 (2023).

[2] Wang, T. et al. Resolution-enhanced multi-core fiber imaging learned on a digital twin for cancer diagnosis. *Neurophotonics* **11**, S11505 (Jan. 2024). Publisher: SPIE.

[3] Wu, J. et al. Learned end-to-end high-resolution lensless fiber imaging towards real-time cancer diagnosis. *Scientific Reports* **12**, 18846 (2022).

[4] Widmann, G. et al. Pre-and post-operative imaging of cochlear implants: a pictorial review. *Insights into Imaging* **11**, 93 (2020).

[5] Fröch, J. E. et al. Real time full-color imaging in a meta-optical fiber endoscope. *eLight* **3**, 13 (Jun. 2023).

[6] Gröger, A. et al. Two-wavelength holographic micro-endoscopy. *Optics Express* **32**, 23687–23701 (Jun 2024).

[7] Sun, J. et al. Lensless fiber endomicroscopy in biomedicine. *PhotoniX* **5**, 18 (2024).

[8] Stibůrek, M. et al. 110 μm thin endo-microscope for deep-brain in vivo observations of neuronal connectivity, activity and blood flow dynamics. *Nature Communications* **14**, 1897 (2023).

[9] Wen, Z. et al. Single multimode fibre for in vivo light-field-encoded endoscopic imaging. *Nature Photonics* **17**, 679–687 (Jul. 2023).

[10] Choi, W. et al. Flexible-type ultrathin holographic endoscope for microscopic imaging of unstained biological tissues. *Nature Communications* **13**, 4469 (Aug. 2022).

[11] Weinberg, G., Weiss, U. & Katz, O. Image scanning lensless fiber-bundle endomicroscopy. *Optics Express* **31**, 37050–37057 (Oct. 2023).

[12] Weinberg, G. et al. Ptychographic lensless coherent endomicroscopy through a flexible fiber bundle. *Optics Express* **32**, 20421–20431 (Jun 2024).

[13] Yeminy, T. & Katz, O. Guidestar-free image-guided wavefront shaping. *Science advances* **7**, eabf5364 (2021).

[14] Lich, J. et al. Single-shot 3d incoherent imaging with diffuser endoscopy. *Light: Advanced Manufacturing* **5**, 218–228 (2024).

[15] Skarsoulis, K. et al. Ptychographic imaging with a fiber endoscope via wavelength scanning. *Optica* **11**, 782–790 (Jun 2024).

[16] Zheng, Y. et al. Single-ended recovery of optical fiber transmission matrices using neural networks. *Communications Physics* **6**, 306 (Oct. 2023).

[17] Eadie, M. et al. Fiber bundle image reconstruction using convolutional neural networks and bundle rotation in endomicroscopy. *Sensors* **23**, 2469 (Feb. 2023).

[18] Sun, J. et al. Quantitative phase imaging through an ultra-thin lensless fiber endoscope. *Light: Science & Applications* **11**, 204 (Jul. 2022).

[19] Sun, J. et al. Calibration-free quantitative phase imaging in multi-core fiber endoscopes using end-to-end deep learning. *Optics Letters* **49**, 342–345 (Jan. 2024).

[20] Thompson, A. J. et al. Adaptive phase compensation for ultracompact laser scanning endomicroscopy. *Optics letters* **36**, 1707–1709 (2011).

[21] Andresen, E. R. et al. Toward endoscopes with no distal optics: video-rate scanning microscopy through a fiber bundle. *Optics letters* **38**, 609–611 (2013).

[22] Koukourakis, N. et al. Investigation of human organoid retina with digital holographic transmission matrix measurements. *Light: Advanced Manufacturing* **3**, 211–225 (2022).

[23] Stasio, N. et al. Light control in a multicore fiber using the memory effect. *Optics express* **23**, 30532–30544 (2015).

[24] Vellekoop, I. M. & Mosk, A. Focusing coherent light through opaque strongly scattering media. *Optics letters* **32**, 2309–2311 (2007).

[25] Scharf, E. et al. Video-rate lensless endoscope with self-calibration using wavefront shaping. *Optics Letters* **45**, 3629–3632 (2020).

[26] Kuschmierz, R. et al. Self-calibration of lensless holographic endoscope using programmable guide stars. *Optics letters* **43**, 2997–3000 (2018).

[27] Badt, N. & Katz, O. Real-time holographic lensless micro-endoscopy through flexible fibers via fiber bundle distal holography. *Nature Communications* **13**, 6055 (2022).

[28] Sivankutty, S. et al. Nonlinear imaging through a fermat's golden spiral multicore fiber. *Optics letters* **43**, 3638–3641 (2018).

[29] El Moussawi, F. et al. Tapered multicore fiber for lensless endoscopes. *ACS photonics* **9**, 2547–2554 (2022).

[30] Tsvirkun, V. et al. Flexible lensless endoscope with a conformationally invariant multi-core fiber. *Optica* **6**, 1185–1189 (2019).

[31] Zolnacz, K. et al. Multicore fiber with thermally expanded cores for increased collection efficiency in endoscopic imaging. *Light: Advanced Manufacturing* **5**, 580–587 (2024).

[32] Kuschmierz, R. et al. Ultra-thin 3d lensless fiber endoscopy using diffractive optical elements and deep neural networks. *Light: Advanced Manufacturing* **2**, 415–424 (2021).

[33] Fontaine, N. K. et al. Laguerre-gaussian mode sorter. *Nature communications* **10**, 1865 (2019).

[34] Trägårdh, J. et al. Label-free cars microscopy through a multimode fiber endoscope. *Optics express* **27**, 30055–30066 (2019).

[35] Morales-Delgado, E. E. et al. Three-dimensional microfabrication through a multimode optical fiber. *Optics express* **25**, 7031–7045 (2017).

[36] Weiss, U. & Katz, O. Two-photon lensless micro-endoscopy with in-situ wavefront correction. *Optics Express* **26**, 28808–28817 (2018).

[37] Kakkava, E. et al. Selective femtosecond laser ablation via two-photon fluorescence imaging through a multimode fiber. *Biomedical optics express* **10**, 423–433 (2019).

[38] Zhao, T. et al. High-speed photoacoustic-guided wavefront shaping for focusing light in scattering media. *Optics Letters* **46**, 1165–1168 (2021).

[39] Schmieder, F., Büttner, L. & Czarske, J. Adaptive laser-induced ultrasound generation using a micro-mirror array spatial light modulator. *Optics Express* **24**, 22536–22543 (Sep. 2016).

[40] Sun, J. et al. Ai-driven projection tomography with multicore fibre-optic cell rotation. *Nature Communications* **15**, 147 (2024).

[41] Tate, T. H. et al. Ultraminiature optical design for multispectral fluorescence imaging endoscopes. *Journal of Biomedical Optics* **22**, 036013 (Mar. 2017).

[42] Small, E. et al. Spectral control of broadband light through random media by wavefront shaping. *Optics Letters* **37**, 3429–3431 (Aug. 2012).

[43] Liu, J. et al. Programmable multiwavelength achromatic focusing and imaging through scattering media. *IEEE Photonics Journal* **10**, 6900811 (Oct. 2018).

[44] Wu, D. et al. Delivering targeted color light through a multimode fiber by field synthesis. *Optics Express* **28**, 19700–19710 (Jun. 2020).

[45] Katz, O. et al. Focusing and compression of ultrashort pulses through scattering media. *Nature Photonics* **5**, 372–377 (May 2011).

[46] Schmieder, F. et al. Two-wavelength computational holography for aberration-corrected simultaneous optogenetic stimulation and inhibition of in vitro biological samples. *Applied Sciences* **12**, 2283 (Feb. 2022).

[47] Shaked, N. T. et al. Label-free biomedical optical imaging. *Nature Photonics* **17**, 1031–1041 (Nov. 2023).

[48] Andresen, E. R. et al. Measurement and compensation of residual group delay in a multi-core fiber for lensless endoscopy. *Journal of the Optical Society of America B* **32**, 1221–1228 (2015).

[49] Vellekoop, I. M. & Mosk, A. Phase control algorithms for focusing light through turbid media. *Optics communications* **281**, 3071–3080 (2008).

[50] Jesacher, A., Bernet, S. & Ritsch-Marte, M. Colour hologram projection with an slm by exploiting its full phase modulation range. *Optics express* **22**, 20530–20541 (2014).

[51] Tsvirkun, V. et al. Widefield lensless endoscopy with a multicore fiber. *Optics Letters* **41**, 4771–4774 (Oct. 2016).

[52] Ding, K. et al. Snapshot spectral imaging: from spatial-spectral mapping to metasurface-based imaging. *Nanophotonics* **13**, 1303–1330 (Mar. 2024).